

Understanding Substituent Effects on ^{29}Si Chemical Shifts and Bonding in Disilynes. A Quantum-Chemical Analysis

Dominik Auer, Martin Kaupp, and Carsten Strohmann*

Institut für Anorganische Chemie, Universität Würzburg,
Am Hubland, 97074 Würzburg, Germany

Received June 17, 2005

The ^{29}Si chemical shifts in substituted disilynes have been analyzed by quantum-chemical studies using a detailed breakdown of paramagnetic contributions into couplings of occupied and virtual canonical molecular orbitals. The results give indications of substituent effects on shielding and confirm the importance of energy denominators in the equation for σ^{P} in symmetrical substituted disilynes ($\text{H}_3\text{SiSiSiSiH}_3$ and $\text{H}_3\text{CSiSiSiCH}_3$) on their chemical shifts. In the unsymmetrical substituted disilyne $\text{H}_3\text{CSiSiSiH}_3$ the energy denominators are identical for both sites and thus cannot explain the widely different chemical shifts. It turns out that the asymmetric charge distribution (reflected in both occupied and virtual MOs and sampled by the PSO matrix elements) allows more efficient couplings at the methyl-substituted silicon side. Furthermore, shielding values in disilynes depend strongly on the size of the trans-bent angle φ , as indicated clearly by analyses of the ^{29}Si chemical shifts in the model $\text{H}_3\text{SiSiSiSiH}_3$ at selected values of φ . Small changes in φ influence the ^{29}Si shielding values appreciably. At lower values of φ , couplings between bonding and virtual MOs exhibit stronger deshielding caused by significantly lower energy denominators.

Multiple bonds between non-first-row main-group elements have long been considered to be unstable. This assumption — known as the “double bond rule” — was disproved by the synthesis and structural characterization of doubly bonded tin–tin,^{1a} silicon–silicon,^{1b} and silicon–carbon^{1c–e} compounds in the late 1970s and early 1980s. In the case of disilenes, more than 50 examples have been successfully synthesized so far,² despite the complexity of their preparation. On the basis of these results and on the predicted stability of disilynes by quantum-chemical studies,³ the synthesis and structural characterization of a related silicon–silicon triple bond was a long-sought goal. Early reports merely indicated the formation of disilynes as intermediates.⁴ The first experimental indication of a stable disilyne was

given by Wiberg in 2002 by NMR analysis (^{29}Si NMR: 91.5 ppm) and mass spectrometry ($\text{M}^+ = \mathbf{1} + \text{O}_2$) of **1**. However, the compound was very sensitive and could not be isolated and characterized further.⁵ In 2004 two groups almost simultaneously reported successful syntheses of compounds with a silicon–silicon triple bond. Wiberg and co-workers confirmed the formation of **1** by NMR analysis and trapping reactions (e.g. **2** + 2 cycloaddition with ethylene),⁶ while Sekiguchi et al. succeeded in completely characterizing disilyne **2** by crystal structure analysis and NMR spectroscopy (cf. Figure 1).⁷

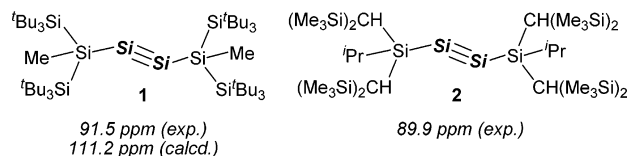


Figure 1. Structures and ^{29}Si NMR shifts of experimentally investigated disilynes.^{6–8}

System **2** exhibits a characteristic trans-bent structure ($\varphi = 137.4^\circ$), which may be rationalized by the CGMT (Carter–Goddard–Malrieu–Trinquier)⁹ donor–

* To whom correspondence should be addressed. E-mail: mail@carsten-strohmann.de.

(1) (a) Goldberg, D. E.; Harris, D. H.; Lappert, M. F.; Thomas, K. *M. J. Chem. Soc., Chem. Commun.* **1976**, 261. (b) West, R.; Fink, M. J.; Michl, J. *Science* **1981**, *214*, 1343. (c) Brook, A. G.; Abdesaken, F.; Gutekunst, B.; Gutekunst, G.; Kallury, R. K. *J. Chem. Soc., Chem. Commun.* **1981**, 191. (d) Brook, A. G.; Nyburg, S. C.; Abdesaken, F.; Gutekunst, B.; Gutekunst, G.; Krishna, R.; Kallury, M. R.; Poon, Y. C.; Chang, Y. M.; Winnie, W. N. *J. Am. Chem. Soc.* **1982**, *104*, 5667. (e) Wiberg, N.; Wagner, G.; Müller, G.; Riede, J. *J. Organomet. Chem.* **1984**, *271*, 381.

(2) (a) Kira, M. *J. Organomet. Chem.* **2004**, *689*, 4475. (b) Baines, K. M.; Samuel, M. S. *Sci. Synth.* **2002**, *4*, 117. (c) Weidenbruch, M. In *Chemistry of Organic Silicon Compounds*; Rappoport, Z., Apeloig, Y., Eds.; Wiley: Chichester, U.K., 2001; Vol. 3, p 391.

(3) (a) Danovich, D.; Ogliaro, F.; Karni, M.; Apeloig, Y.; Cooper, D. L.; Shaik, S. *Angew. Chem., Int. Ed.* **2001**, *40*, 4023 and references therein. (b) Kobayashi, K.; Takagi, N.; Nagase, S. *Organometallics* **2001**, *20*, 234 and references therein. (c) For a review on the bonding in heavier main-group acetylene analogues see: Power, P. P. *Chem. Commun.* **2003**, 2091 and references therein.

(4) (a) Sekiguchi, A.; Zigler, S. S.; West, R.; Michl, J. *J. Am. Chem. Soc.* **1986**, *108*, 4241. (b) Pietschnig, R.; West, R.; Powell, D. R. *Organometallics* **2000**, *19*, 2724.

(5) Wiberg, N.; Niedermayer, W.; Fischer, G.; Nöth, H.; Suter, M. *Eur. J. Inorg. Chem.* **2002**, 1066.

(6) Wiberg, N.; Vasisht, S. K.; Fischer, G.; Mayer, P. *Z. Anorg. Allg. Chem.* **2004**, *630*, 1823.

(7) Sekiguchi, A.; Kinjo, R.; Ichinohe, M. *Science* **2004**, *305*, 1755.

(8) Takagi, N.; Nagase, S. *Eur. J. Inorg. Chem.* **2002**, 2775.

(9) (a) Carter, E. A.; Goddard, W. A., III. *J. Phys. Chem.* **1986**, *90*, 998. (b) Trinquier, G.; Malrieu, J. P. *J. Am. Chem. Soc.* **1987**, *109*, 5303. (c) Malrieu, J. P.; Trinquier, G. *J. Am. Chem. Soc.* **1989**, *111*, 5916. (d) Trinquier, G.; Malrieu, J. P. *J. Phys. Chem.* **1990**, *94*, 6184.

(e) Trinquier, G. *J. Am. Chem. Soc.* **1990**, *112*, 2130.

acceptor model.¹⁰ The ²⁹Si NMR resonance signals of the central silicon atoms in **2** appear at 89.9 ppm and are in good agreement with the values observed for **1**. In addition, quantum-chemical studies on **1** indicated a trans-bent angle of 148.0° and ²⁹Si NMR shifts of 111.2 ppm for the central silicon atoms.⁸

²⁹Si NMR spectroscopy is the most important diagnostic tool for the characterization of disilynes such as **1** and **2**. An initial interpretation of the ²⁹Si NMR chemical shifts of disilynes was obtained by comparison with acetylene systems.⁷ As an understanding on the basis of this comparison is not sufficient, we decided to analyze the ²⁹Si NMR chemical shifts in more detail. In this context an important question is how sensitive the ²⁹Si NMR shifts in disilynes are to changes of the trans-bent angle φ .¹¹

Theoretical Background

The proper basis for interpretation is provided by Ramsey's equation,¹² i.e., by second-order perturbation theory (unless relativistic effects become important¹³). Except for proton NMR, it is usually assumed that changes in chemical shifts are due to changes in paramagnetic shielding, σ^p . When using Hartree–Fock or density functional theory (DFT), one may rewrite the term for paramagnetic shielding in Ramsey's equation as a double sum over occupied and virtual molecular orbitals ϕ_k and ϕ_a , respectively (u and v represent Cartesian components):¹⁴

$$\sigma_{N,uv}^p = -\frac{2}{c^2} \sum_k^{\text{occ}} \sum_a^{\text{vac}} \frac{\langle \phi_k | l_{O,u} | \phi_a \rangle \cdot \langle \phi_a | l_{N,v} \cdot r_N^{-3} | \phi_k \rangle}{\Delta E_{k-a}} + \text{cc} \quad (1)$$

The two matrix elements in the numerators reflect interactions with (a) the external magnetic field ("orbital Zeeman term", OZ) and (b) the magnetic moment of the nucleus in question (the paramagnetic nuclear spin electron orbit term, PSO).¹⁴ On the same grounds as detailed in our previous study of disilene chemical shifts,¹⁵ our analysis will be based on a gradient-corrected density functional calculation with a common gauge origin (CGO) at the midpoint of the two central silicon atoms.¹⁶ As previously described, this method of analysis allows a breakdown of σ^p into individual contributions from occupied and unoccupied molecular orbitals (MOs) within a DFT framework.¹⁵

(10) For heavier main-group acetylene analogues another bonding model based on a molecular orbital approximation is known. This model involves mixing of canonical MOs and is more flexible concerning bond lengths and bond orders. For a detailed description, including MO plots, see ref 3c.

(11) During revision of this work we became aware of the following contribution by M. Karni, which also considers effects of structural parameters on the ²⁹Si chemical shifts in disilynes: Karni, M.; Apeloig, Y.; Takagi, N.; Nagase, S. *Organometallics* **2005**, *24*, 6319.

(12) Ramsey, N. F. *Phys. Rev.* **1950**, *78*, 699.

(13) Kaupp, M.; Malkina, O. L.; Malkin, V. G.; Pyykkö, P. *Chem. Eur. J.* **1998**, *4*, 118 and references therein.

(14) l_O represents the angular momentum around the gauge origin of the external vector potential due to the external magnetic field, and l_N represents the angular momentum around the nucleus in question. Equation 1, which refers to a common gauge origin, uses cgs-based atomic units, and c is the speed of light. Throughout this work, OZ matrix elements will be provided in mHartree/Zeman (1 Hartree = 27.2116 eV, 1 Zeeman = 2.4×10^5 T) and PSO matrix elements in 10^{-3} Zeeman.

(15) Auer, D.; Strohmam, C.; Arbusnikov, A. V.; Kaupp, M. *Organometallics* **2003**, *22*, 2442 and references therein.

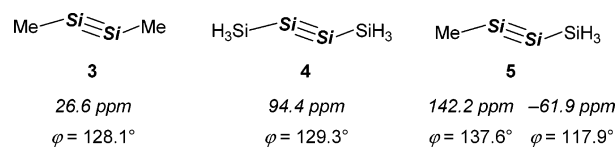


Figure 2. Calculated ²⁹Si chemical shifts (BP86-GIAO/IGLO-III/MP2/6-31+G(d)) and trans-bent angles φ (MP2/6-31+G(d)) of model systems **3–5**.

Computational Details

Structure optimizations and harmonic vibrational frequency analyses (to establish the nature of stationary points on the potential energy surface) were performed at the MP2/6-31+G(d) level, using the Gaussian98 program package.¹⁷ All model systems were optimized without symmetry. Chemical shifts were initially calculated with Gaussian98 at the BP86-GIAO gradient-corrected DFT level,¹⁸ using extended IGLO-III basis sets.¹⁹ Calculated absolute shieldings σ were converted to relative shifts δ via calculated shieldings for tetramethylsilane (TMS) at the same level ($\sigma_{\text{calc}}(\text{Si})$ 327.5 ppm for the BP86-GIAO/IGLO-III/MP2/6-31+G(d) level). Isotropic shieldings and shifts are the average of the three principal tensor components.

Subsequent analyses of the individual contributions to σ^p for **3–5** were carried out at the BP86-CGO/IGLO-III level (Figure 2). We used Kohn–Sham orbitals obtained with Gaussian98 and transferred them to the in-house property program MAG-ReSpect²⁰ by an interface routine.²¹ MAG-ReSpect²⁰ allows the detailed analysis of individual contributions to nuclear shieldings as discussed above.

Natural population analyses²² employed the built-in NBO-3.0 subroutines of the Gaussian98 program and were performed on the BP86/IGLO-III wave functions.

Results and Discussion

Early quantum-chemical studies on the Si₂H₂ model system indicated a trans-bent structure as a reasonable structure proposal for disilynes.²³ This was confirmed by calculations on larger, substituted systems, e.g. on **1**,⁸ and also by crystal structure analysis on **2**.⁷ Our

(16) For a recent discussion of advantages and disadvantages of different choices of gauge and different analysis method for nuclear shieldings, see: Kaupp, M. In *Calculation of NMR and EPR Parameters: Theory and Applications*; Kaupp, M., Bühl, M., Malkin, V. G., Eds.; Wiley-VCH: Weinheim, Germany, 2004; p 293ff.

(17) Frisch, M. J.; Trucks, G. W.; Schlegel, H. B.; Scuseria, G. E.; Robb, M. A.; Cheeseman, J. R.; Zakrzewski, V. G.; Montgomery, J. A., Jr.; Stratmann, R. E.; Burant, J. C.; Dapprich, S.; Millam, J. M.; Daniels, A. D.; Kudin, K. N.; Strain, M. C.; Farkas, O.; Tomasi, J.; Barone, V.; Cossi, M.; Cammi, R.; Mennucci, B.; Pomelli, C.; Adamo, C.; Clifford, S.; Ochterski, J.; Petersson, G. A.; Ayala, P. Y.; Cui, Q.; Morokuma, K.; Malick, D. K.; Rabuck, A. D.; Raghavachari, K.; Foresman, J. B.; Cioslowski, J.; Ortiz, J. V.; Stefanov, B. B.; Liu, G.; Liashenko, A.; Piskorz, P.; Komaromi, I.; Gomperts, R.; Martin, R. L.; Fox, D. J.; Keith, T.; Al-Laham, M. A.; Peng, C. Y.; Nanayakkara, A.; Gonzalez, C.; Challacombe, M.; Gill, P. M. W.; Johnson, B. G.; Chen, W.; Wong, M. W.; Andres, J. L.; Head-Gordon, M.; Replogle, E. S.; Pople, J. A. *Gaussian 98*, revision A.9; Gaussian, Inc.: Pittsburgh, PA, 1998.

(18) (a) Wolinski, K.; Hinton, J. F.; Pulay, P. *J. Am. Chem. Soc.* **1990**, *112*, 8251 and references therein; (b) Becke, A. D. *Phys. Rev. A: Gen. Phys.* **1988**, *38*, 3098. (c) Perdew, J. P. *Phys. Rev. B: Condens. Matter* **1986**, *33*, 8822.

(19) Kutzelnigg, W.; Fleischer, U.; Schindler, M. In *NMR-Basic Principles and Progress*; Diehl, P., Fluck, E., Günther, H., Kosfeld, R., Eds.; Springer-Verlag: Heidelberg, Germany, 1990; Vol. 23, p 165.

(20) Malkin, V. G.; Malkina, O. L.; Reviakine, R.; Arbusnikov, A. V.; Kaupp, M.; Schimmelpennig, B.; Malkin, I.; Helgaker, T.; Ruud, K. *MAG-ReSpect*, version 1.1; 2003.

(21) (a) Reviakine, R. *Gaussian-to-MAG interface*, version 1.0; 2002. (b) Kaupp, M.; Reviakine, R.; Malkina, O. L.; Arbusnikov, A.; Schimmelpennig, B.; Malkin, V. G. *J. Comput. Chem.* **2002**, *23*, 794.

(22) (a) Reed, A. E.; Weinhold, F. *J. Chem. Phys.* **1985**, *83*, 1736. (b) Reed, A. E.; Curtiss, L. A.; Weinhold, F. *Chem. Rev.* **1988**, *88*, 899.

structure optimizations of model systems **3**–**5** (cf. Table 1 in the Supporting Information for structural parameters²⁴) are in line with these results. In analogy to recent computations on disilene model systems,¹⁵ the unsymmetrical disilyne **5** is significantly more bent at the silyl-substituted center (Si(2)). This can be rationalized by considering the natural charge distribution for **5** (cf. Figure 3a): the silyl-substituted “silylyne” fragment is negatively charged. According to the CGMT donor–acceptor model,⁹ the methyl-substituted fragment acts more as a donor, while the silyl-substituted fragment is a net electron acceptor. This behavior may be understood by electrostatic preferences, as the unequal charge transfer leads to a favorable alternation of negative and positive charges. In consequence the silyl-substituted side is more bent ($\varphi = 117.9^\circ$) than the methyl-substituted side ($\varphi = 137.6^\circ$).

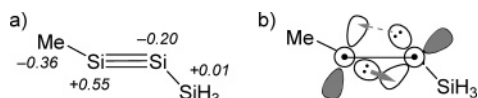


Figure 3. (a) Calculated natural charges for central silicon atoms and substituents in **5**. The silylyne fragment charges are as follows: MeSi, +0.19; H₃SiSi, -0.19. (b) Approximate bonding scheme for **5** (following the CGMT model) with two donor–acceptor bonds (indicated by arrows) and one π bond between p orbitals (indicated by the line).^{9,10}

Comparison of BP86-CGO/IGLO-III and BP86-GIAO/IGLO-III shieldings (cf. Table 1) shows notable but acceptable differences. In particular, all trends and substituent effects are reproduced at the common-gauge level. This allows us to perform the shielding analysis of models **3**–**5** at the BP86-CGO/IGLO-III/MP2/6-31+G(d) level. Contributions to σ^p were broken down into individual terms of eq 1 related in each single case to the coupling of one occupied with one virtual MO. We note that for all three models the dominant contributions arise from couplings of the three highest occupied molecular orbitals (cf. Figures 4 and 5 and Tables 2, 3, and 5 for isosurface plots) to virtual MOs. For reasons of clarity, Tables 2, 3, and 5 generally list only the major contributions to σ^p .

Table 1. Influence of Gauge Treatment on ²⁹Si Shielding Tensors^a

model	gauge	σ_1	σ_2	σ_3	σ_{iso}
3	GIAO	-43.7	159.9	786.5	300.9
	CGO	-36.4	162.4	785.8	303.9
4	GIAO	-155.7	52.3	802.6	233.1
	CGO	-124.8	79.5	805.4	253.4
5 (Si1)	GIAO	-209.4	30.3	735.1	185.3
	CGO	-195.2	37.1	736.6	192.8
5 (Si2)	GIAO	86.8	228.4	852.9	389.4
	CGO	110.7	247.5	854.6	404.3

^a MAG-ReSpect results at the BP86/IGLO-III level in ppm.

In **3**, the $\sigma(\text{Si}-\text{C})$ and $\sigma(\text{Si}=\text{Si})$ bonding MO 21 dominates contributions to σ^p . Magnetic couplings of this

MO are distributed over a series of appropriate combinations. The largest involve virtual MOs 24 and 25. In general, a large contribution of a coupling to σ^p arises when (a) the energy denominator is sufficiently small and (b) both matrix elements in the numerator are sufficiently large (cf. eq 1). The latter requires that angular momentum (present in both OZ and PSO operators) transforms an occupied MO to a form that overlaps well with the appropriate unoccupied MO. This corresponds to a paramagnetic ring current in the plane containing the two MOs involved, with the corresponding major contribution to σ^p pointing perpendicular to this plane and therefore along the axis of rotation.

In model system **3** this can be illustrated easily, e.g. by comparing MO 21 to the LUMO 24. Rotation of MO 21 around the σ_1 axis (perpendicular to the plane of the two silicon and two carbon atoms; cf. Figure 4) results in a transformed MO that matches nicely with the LUMO 24. As the corresponding energy denominator is relatively small ($\Delta E(21 \rightarrow 24)$: -4.30 eV; cf. Table 2) this coupling exhibits a significant deshielding contribution along the z axis (σ_1 ; cf. Table 2), making it the overall largest individual coupling in **3**. However, MO 21 also contributes strongly along the y axis (σ_2 ; cf. Table 2), by a good match with the LUMO+1 25, despite the relatively large energy denominator (-6.19 eV; cf. Table 2). Both couplings may be described more or less as $\sigma-\pi^*$ couplings (MO 24 is not a pure π^* -type MO but has a slightly more complicated character), consistent with previous studies on doubly and triply bonded compounds.^{15,25}

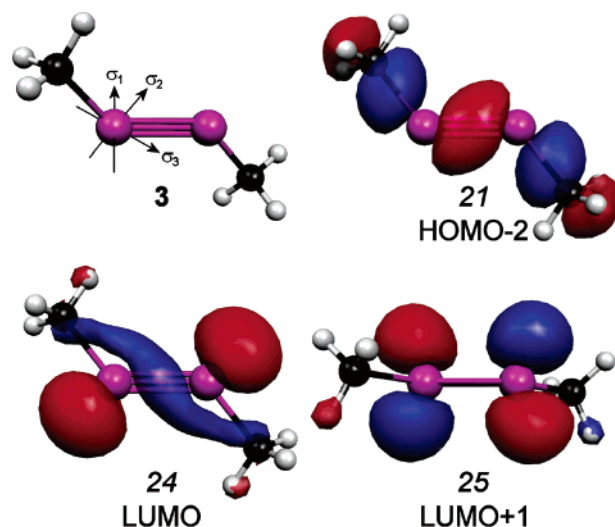


Figure 4. Isosurface plots (± 0.05 au) of selected MOs (for reasons of clarity MO 25 is displayed after rotation around the Si–Si axis) for model **3**.²⁶

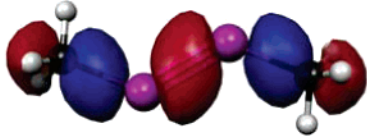
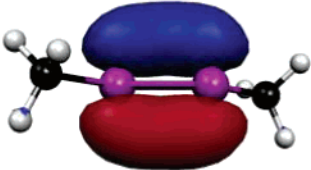
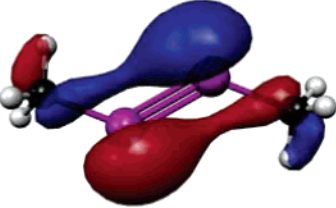
In disilyldisilyne (**4**) the coupling of the corresponding $\sigma(\text{Si}-\text{Si})$ and $\sigma(\text{Si}=\text{Si})$ bonding MO 29 with LUMO 32 (Table 3) is larger and thus to a large extent is responsible for the more pronounced deshielding (again via σ_1). The virtual MO 32 involved in this coupling

(23) (a) Lischka, H.; Köhler, H. *J. Am. Chem. Soc.* **1983**, *105*, 6646. (b) Binkley, J. S. *J. Am. Chem. Soc.* **1984**, *106*, 603. For a summary on the history of quantum-chemical calculations on the stability of heavy-atom group 14 analogues of acetylene E₂H₂ and recent results to this field see: Lein, M.; Krapp, A.; Frenking, G. *J. Am. Chem. Soc.* **2005**, *127*, 6290 and references therein.

(24) For other calculated Si=Si bond distances see also: Pyykkö, P.; Riedel, S.; Patzschke, M. *Chem. Eur. J.* **2005**, *11*, 3511.

(25) (a) West, R.; Cavalieri, J. D.; Buffy, J. J.; Fry, C.; Zilm, K. W.; Duchamp, J. C.; Kira, M.; Iwamoto, T.; Mueller, T.; Apeloig, Y. *J. Am. Chem. Soc.* **1997**, *119*, 4972. (b) Zilm, K. W.; Conlin, R. T.; Grant, D. M.; Michl, J. *J. Am. Chem. Soc.* **1980**, *102*, 6672. (c) Beeler, A. J.; Orendt, A. M.; Grant, D. M.; Cutts, P. W.; Michl, J.; Zilm, K. W.; Downing, J. W.; Facelli, J. C.; Schindler, M. S.; Kutzelnigg, W. *J. Am. Chem. Soc.* **1984**, *106*, 7672.

Table 2. Analysis of the Major Contribution to σ^p Values of **3**^a

orbital/no. ^a	contribn.	couplings to MO ^b	dir ^c	ΔE^d	OZ	PSO
 21	-416.8	24: -224.2	σ_1	-4.30	3.76	7.06
		25: -197.4	σ_2	-6.19	4.37	7.71
		27: -8.4	σ_1	-8.35	1.10	1.76
		rest: +13.2	-	-	-	-
 22	-65.2	28: -42.1	σ_1	-6.52	2.86	2.67
		29: -17.9	σ_1	-7.40	1.69	2.22
		rest: -5.2	-	-	-	-
 23	-64.2	26: -50.1	σ_3	-3.41	1.78	3.24
		28: -12.8	σ_2	-5.33	0.90	3.48
		29: +14.6	σ_2	-6.21	-1.01	2.50
		rest: -15.9	-	-	-	-

^a Isosurface plots (± 0.05 au) of selected MOs (for reasons of clarity MO 22 is displayed after rotation around the Si–Si axis). Shielding contributions are given in ppm, OZ matrix elements in mHartree/Zeeaman, and PSO matrix elements in 10^{-3} Zeeman. ^b Selection of largest contributions (up to three). ^c Main direction(s) to which this coupling contributes. ^d $\Delta E = \epsilon_a - \epsilon_b$ in eV.

resembles the virtual MO 24 in dimethyldisilyne (**3**) (and MO 33 is analogous to MO 25 in the latter molecule). While the product of the OZ and PSO matrix elements for this coupling is also slightly larger in **4** than in **3**, the main difference is caused by the smaller energy denominator ($\Delta E(21 \rightarrow 24)$ in **3**, -4.30 eV; $\Delta E(29 \rightarrow 32)$ in **4**, -3.39 eV; see also Tables 2 and 3). This behavior is due to the higher energy of MO 29 (-7.29 eV) and lower energy of MO 32 (-3.89 eV) in **4** when compared to the energies of MOs 21 (-7.73 eV) and 24 (-3.43 eV) in **3**. The fact that the silyl-substituted system **4** exhibits a smaller energy denominator is consistent with the results from prior work on disilenes by West et al.²⁵ and by us.¹⁵ Closer comparison of Tables 2 and 3 shows that the 29 \rightarrow 32 and 29 \rightarrow 33 couplings in **4** are enhanced (along σ_1 and σ_2) in comparison to the analogous 21 \rightarrow 24 and 21 \rightarrow 25 couplings in **3**. However, as contributions to σ_3 are reduced, σ_{iso} differs less than σ_1 and σ_2 might suggest (Table 1).

We further emphasize that changes in the trans-bent angle φ influence the paramagnetic shielding σ^p significantly. A lower value of 110° results in significantly decreased σ values, while a more “linear” structure ($\varphi = 160^\circ$) causes the opposite effect (cf. Table 4). This trend is dominated by the 29 \rightarrow 32 and 29 \rightarrow 33 couplings, which exhibit clearly smaller energy denominators upon a decrease of φ to 110° (cf. Table 5). An increase of φ to 160° affects the MO energies appreciably (e.g. MO 29

is lowered while MO 32 rises notably; see ref 3c for a thorough discussion of the effects of the trans-bent angle on MO energies). Furthermore, the contributions by the 29 \rightarrow 32 and 29 \rightarrow 33 couplings start to converge toward each other as the virtual MOs 32 and 33 approach degeneracy (Table 6). Obviously, at $\varphi = 160^\circ$ the virtual MOs 32 and 33 begin to resemble the π^* virtual orbitals in linear triply bonded systems such as acetylene.

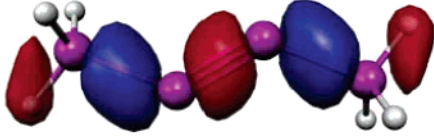
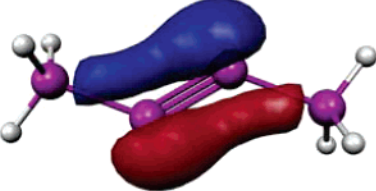
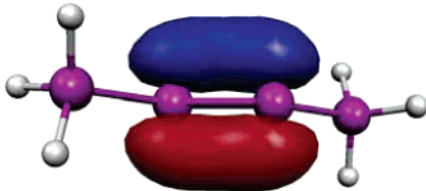
The situation changes significantly for the unsymmetrical 1-silyl-2-methyldisilyne (**5**). The large difference in isotropic shifts of the two silicon atoms is most obvious: the silicon center on the silyl-substituted side (Si(2)) is over 200 ppm more shielded than that on the methyl-substituted side (Si(1)) (cf. Table 7). In comparison to the corresponding sites in the symmetrical systems **3** or **4**, the methyl-substituted Si(1) is roughly 110 ppm more deshielded, while the silyl-substituted Si(2) is roughly 150 ppm more shielded.

Table 7 shows clearly that the major differences in shielding are caused by the couplings of MO 25 to higher virtual orbitals.²⁷ However, one may not argue via different energy denominators for the different sites, as

(26) Flükiger, P.; Lüthi, H. P.; Portmann, S.; Weber, J. *MOLEKEL* 4.3; Swiss Center for Scientific Computing, Manno, Switzerland, 2000–2002.

(27) The effect is additionally enhanced by contributions of lower lying bonding MOs. For a detailed overview on all effects by contributing MOs, see the Supporting Information.

Table 3. Analysis of the Major Contribution to σ^p Values of 4^a

orbital/no. ^a	contribn.	couplings to MO ^b	dir ^c	ΔE^d	OZ	PSO
 29	-519.8	32: -308.9	σ_1	-3.39	4.21	6.87
		33: -226.3	σ_2	-4.50	4.01	7.02
		35: +21.3	σ_1	-7.17	-2.30	1.82
		rest: -5.9	-	-	-	-
 30	-48.4	36: -30.3	σ_1	-5.99	2.42	2.07
		39: +6.6	σ_1	-6.37	-0.72	1.60
		42: -34.8	σ_1	-7.52	2.11	3.54
		rest: +10.1	-	-	-	-
 31	-58.0	34: -16.3	σ_3	-3.51	0.55	3.01
		36: -39.3	σ_2	-5.12	2.29	2.54
		39: +9.3	σ_2	-5.50	-0.80	2.90
		rest: -11.7	-	-	-	-

^a Isosurface plots (± 0.05 au) of selected MOs (for reasons of clarity MO 31 is displayed after rotation around the Si-Si axis). Shielding contributions are given in ppm, OZ matrix elements in mHartree/Zee-man, and PSO matrix elements in 10^{-3} Zeeman. ^b Selection of largest contributions (up to three). ^c Main direction(s) to which this coupling contributes. ^d $\Delta E = \epsilon_a - \epsilon_k$ in eV.

Table 4. Influence of the Trans-Bent Angle φ on the σ Values in 4

trans-bent angle φ	σ	trans-bent angle φ	σ
110.0	112.8	140.0	295.7
120.0	203.4	150.0	333.3
129.3	253.4	160.0	366.5

Table 5. Analysis of the Major Contribution to σ^p Values of 4 at 110°^a

orbital no.	contribn	couplings to MO ^b	dir ^c	ΔE^d	OZ	PSO
29	-653.1	32: -433.2	σ_1	-2.23	3.91	6.82
		33: -265.3	σ_2	-4.07	4.10	7.27
		36: +42.9	σ_1	-6.53	-2.71	2.88
		rest: +2.5				
30	-62.5	35: -69.6	σ_1	-6.16	3.80	3.17
		rest: +7.1				
31	-56.9	34: -6.9	σ_{23}	-4.17	0.29	2.82
		35: -34.1	σ_3	-4.90	1.40	3.76
		38: -6.5	σ_{23}	-5.57	1.47	1.20
		rest: -9.4				

^a Shielding contributions are given in ppm, OZ matrix elements in mHartree/Zee-man, and PSO matrix elements in 10^{-3} Zeeman. ^b Selection of largest contributions (up to three). ^c Main direction(s) to which this coupling contributes. ^d $\Delta E = \epsilon_a - \epsilon_k$ in eV.

both the interacting orbitals and their corresponding energy denominators are identical. Even the OZ matrix elements are identical (they describe the interaction of the MOs with the external magnetic field), and hence, we have to focus on variations in the PSO matrix

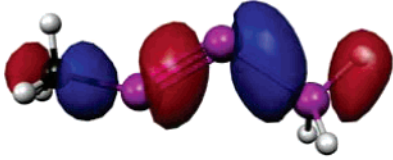
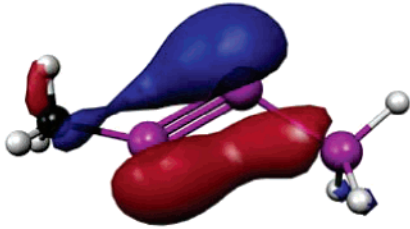
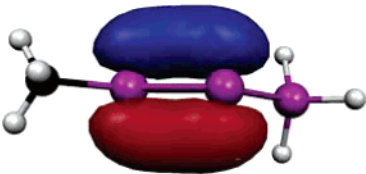
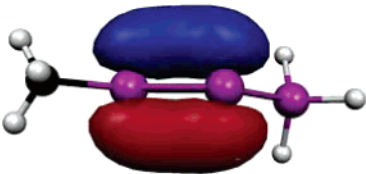
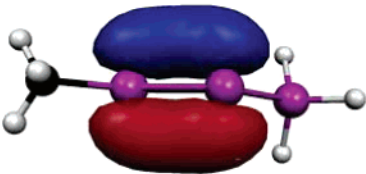
Table 6. Analysis of the Major Contribution to σ^p Values of 4 at 160°^a

orbital no.	contribn	couplings to MO ^b	dir ^c	ΔE^d	OZ	PSO
29	-462.7	32: -240.8	σ_1	-4.81	4.58	6.97
		33: -218.0	σ_2	-4.98	4.31	6.95
		rest: -3.9				
30	-25.6	38: +11.9	σ_1	-5.36	-1.96	0.90
		42: -30.7	σ_1	-7.37	1.91	3.26
		rest: -6.8				
31	-37.2	34: -17.8	σ_{23}	-2.57	0.55	2.33
		35: -23.5	σ_{23}	-5.10	1.85	1.83
		38: +11.9	σ_2	-5.19	-1.70	1.12
		rest: -7.8				

^a Shielding contributions are given in ppm, OZ matrix elements in mHartree/Zee-man, and PSO matrix elements in 10^{-3} Zeeman. ^b Selection of largest contributions (up to three). ^c Main direction(s) to which this coupling contributes. ^d $\Delta E = \epsilon_a - \epsilon_k$ in eV.

element. The difference between the contributions from MO 25 for the two sites is roughly 136 ppm. Sizable differences in the contributions from the π -bonding MOs 26 and HOMO 27 cancel largely (cf. Table 7). Obviously, the shapes of MO 25 and of the corresponding virtual MOs allow overall more efficient couplings (after rotation of MO 25 around σ_1 or σ_2 , respectively) at the methyl-substituted silicon (Si(1)) site. This reflects the unsymmetrical charge distribution (cf. Figure 3) and the related polarizations of both occupied and virtual MOs (see Table 7 and Figure 5). Similar results have been obtained for unsymmetrically substituted disilynes.¹⁵ In

Table 7. Analysis of the Major Contribution to σ^p Values of 5^a

orbital/no. ^a	side	contribn.	couplings to MO ^c	dir ^c	ΔE	OZ	PSO
 25	Si(1)	-476.6	28: -240.5	σ_1	-3.76	3.63	6.86
			29: -178.3	σ_2	-5.23	3.63	7.09
			32: -17.7	σ_1	-7.87	3.01	1.27
			34: -23.8	σ_2	-8.30	2.55	2.15
			rest: -16.3	-	-	-	-
 26	Si(1)	-23.3	28: +13.1	σ_1	-2.21	-0.22	3.60
			29: +14.2	σ_{23}	-3.68	-0.43	6.88
			31: -20.1	σ_1	-5.94	1.77	1.87
			41: -24.0	σ_1	-8.65	1.14	5.02
			rest: -6.5	-	-	-	-
 27	Si(1)	-84.4	28: -19.1	σ_1	-2.21	0.22	5.21
			29: -14.3	σ_{23}	-3.68	0.43	6.68
			31: -20.9	σ_1	-5.94	1.77	1.93
			35: -48.2	σ_1	-7.12	2.11	4.49
			rest: +21.7	-	-	-	-
 27	Si(2)	-37.0	28: -21.6	σ_{23}	-1.17	0.18	8.41
			30: -32.8	σ_{23}	-3.52	0.95	3.59
			31: -7.8	σ_{23}	-4.91	1.19	2.21
			rest: -22.2	-	-	-	-
			28: +9.7	σ_{23}	-1.17	-0.18	7.92
 27	Si(2)	-37.0	30: -18.1	σ_{23}	-3.52	0.95	2.85
			31: -31.5	σ_{23}	-4.91	1.19	3.58
			rest: -2.9	-	-	-	-

^a Isosurface plots (± 0.05 au) of selected MOs (for reasons of clarity MO 27 is displayed after rotation around the Si-Si axis). Shielding contributions are given in ppm, OZ matrix elements in mHartree/Zeeaman, and PSO matrix elements in 10^{-3} Zeeman. ^b Selection of largest contributions (up to three). ^c Main direction(s) to which this coupling contributes. ^d $\Delta E = \epsilon_a - \epsilon_b$ in eV.

the latter case, the analysis was slightly more straightforward, as a smaller number of virtual orbitals were involved. Here we see sizable differences between the two sites for contributions, not only from the lowest lying π^* -type MOs 28 and 29 but also from a number of higher lying virtual MOs. Nevertheless, the predomi-

nance of the PSO matrix elements shows beyond doubt that it is the polarization of the charge distribution toward Si(2) that enhances the σ^p contributions at the Si(1) site. The positive charge at Si(1) is reflected in a larger r^{-3} factor. Parts of the differences between Si(1) and Si(2) shieldings are due to the positive sign of the

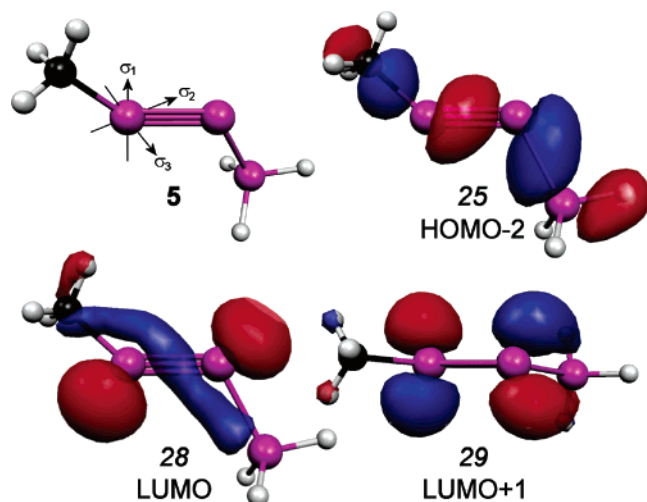


Figure 5. Isosurface plots (± 0.05 au) of selected MOs (for reasons of clarity MO 29 is displayed after rotation around the Si–Si axis) for model **5**.²⁶

25 \rightarrow 31 and 25 \rightarrow 32 couplings (as well as of remaining smaller contributions) for the Si(2) site, whereas similar contributions on the Si(1) site are all negative. Such positive contributions are generally due to strongly off-center couplings. The virtual MOs involved (not shown) are largely delocalized between the Si(2) center and its silyl substituent: i.e., they reflect also the polarity of the Si \equiv Si bond.

Conclusions

Detailed quantum-chemical analyses of the ²⁹Si chemical shifts in substituted disilynes have allowed the rationalization of substituent effects on the shieldings of the central silicon centers. The results confirm the

importance of energy denominators in the equation for σ^p (eq 1) for the shifts in symmetrically substituted disilynes such as **3** and **4**. Furthermore, the shielding values depend strongly on the size of the trans-bent angle φ . Small changes in φ have a significant influence on the ²⁹Si shielding values. At lower values of φ , couplings between bonding and virtual MOs exhibit more deshielding because of significantly lower energy denominators.

In unsymmetrically substituted disilynes the energy denominators are identical for both sites and thus cannot explain the widely different chemical shifts. It turns out that the asymmetric charge distribution, which is reflected in both occupied and virtual MOs and is sampled by the PSO matrix elements, allows more efficient couplings at the methyl-substituted silicon side.

The rationalization of the ²⁹Si shifts in both symmetrical and unsymmetrical disilynes by this MO-by-MO analysis will hopefully aid in future experimental characterizations of further related systems.

Acknowledgment. This work was supported by the Institut für Anorganische Chemie Würzburg, the Deutsche Forschungsgemeinschaft (Project KA1187/5-1), and the DFG Research Training Group 690: Electron Density. D.A. thanks the Research Training Group 690 for the grant of a scholarship. We are grateful to J. Asher for technical assistance.

Supporting Information Available: Tables giving structural parameters, standard orientation, total energies, and the calculated shielding tensors for Si as well as MO contributions to σ and σ^p of disilyne systems **3–5** and further information on the natural population analysis of **5**. This material is available free of charge via the Internet at <http://pubs.acs.org>.

OM050499B